

# RSC Advances



This is an *Accepted Manuscript*, which has been through the Royal Society of Chemistry peer review process and has been accepted for publication.

*Accepted Manuscripts* are published online shortly after acceptance, before technical editing, formatting and proof reading. Using this free service, authors can make their results available to the community, in citable form, before we publish the edited article. This *Accepted Manuscript* will be replaced by the edited, formatted and paginated article as soon as this is available.

You can find more information about *Accepted Manuscripts* in the [Information for Authors](#).

Please note that technical editing may introduce minor changes to the text and/or graphics, which may alter content. The journal's standard [Terms & Conditions](#) and the [Ethical guidelines](#) still apply. In no event shall the Royal Society of Chemistry be held responsible for any errors or omissions in this *Accepted Manuscript* or any consequences arising from the use of any information it contains.

Cite this: DOI: 10.1039/c0xx00000x

www.rsc.org/xxxxxx

## ARTICLE TYPE

## 1D Nanofiber Composites of Perylene Diimides for Visible-light-driven Hydrogen Evolution from Water

Shuai Chen<sup>a,b</sup>, Daniel L. Jacobs<sup>c</sup>, Jingkun Xu<sup>a</sup>, Yingxuan Li<sup>a</sup>, Chuanyi Wang<sup>\*a</sup>, Ling Zang<sup>\*c</sup>

Received (in XXX, XXX) Xth XXXXXXXXX 20XX, Accepted Xth XXXXXXXXX 20XX

DOI: 10.1039/b000000x

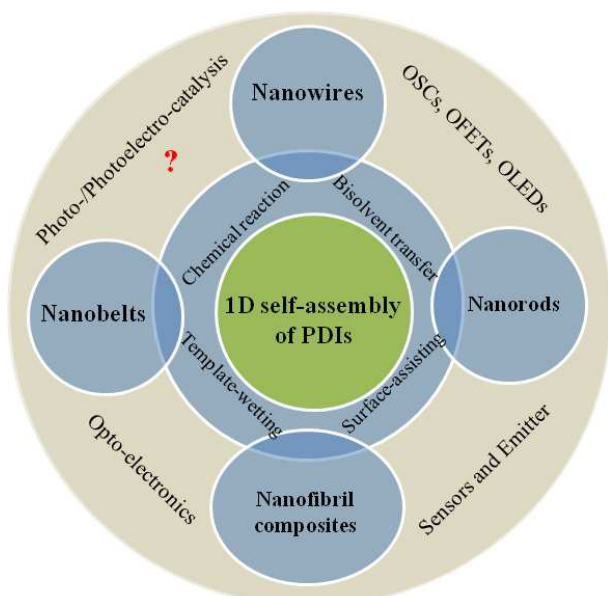
A series of novel nanocomposites structures have been fabricated by in-situ deposition of TiO<sub>2</sub> layers and/or a co-catalyst (Pt) on one-dimensional (1D) self-assembled nanofibers of perylene diimide derivatives (PDIs). The PDIs molecules were functionalized with dodecyl and/or phenylamino groups to compare the effect of nanofiber morphology and intramolecular charge transfer on the photocatalytic performance, respectively. Under visible-light irradiation ( $\lambda > 420$  nm), hydrogen production for all composite systems has been detected through photocatalytic water splitting in aqueous solutions with sacrificial reagent methanol or triethanolamine, proving the applicability of organic nanofibers in photocatalytic system. Compared to the well-defined nanofibril morphology obtained from dodecyl-substituted PDI molecules, donor-accepter type PDIs attached with electron-rich phenylamino moieties show much improved photocatalytic activity due to efficient inter- and intra-molecular charge transfer. This work provides insight into the role of molecular design and nanomorphology of organic semiconductor materials in the field of photocatalysis.

## Introduction

Semiconductor-based photocatalytic splitting of water utilizing solar irradiation has been recognized to be among the most ideal approaches for a clean and renewable energy source.<sup>1-7</sup> Unlike other solar energy technologies (photovoltaic and photothermal) where storing the converted energy can be complicated, solar water splitting stores the energy in stable chemical bonds (hydrogen and oxygen) which can then be used as a fuel for on demand energy. Hydrogen is considered an ideal clean and renewable fuel as the high energy capacity can be converted and collected through either combustion or fuel cell systems with water as the only by-product. However, despite four decades of research since the initial discovery of photocatalytic water splitting, low photoconversion efficiency limits its use in practical applications.<sup>8,9</sup> To realize cheap and efficient solar water splitting, the photocatalytic materials should exhibit strong visible light absorption to match the solar spectrum ( $E_g < 3$  eV), suitable energy levels and bandgap for oxidation and reduction of water to O<sub>2</sub> and H<sub>2</sub> respectively ( $E_g > 1.23$  eV), efficient charge separation to limit the back reaction of H<sub>2</sub> and O<sub>2</sub> to water and should be composed of inexpensive and abundant materials.<sup>1-3</sup> Typical photocatalytic systems often use large bandgap metal oxides that suffer from poor visible light absorption or expensive sensitizing dyes that may not be photostable.<sup>10-12</sup> Similarly, fast charge recombination in most suitable semiconductors occurs much faster than the redox reactions of water, resulting in poor quantum yields.<sup>4,6</sup> Additionally, traditional inorganic semiconductors (typically, TiO<sub>2</sub>)<sup>2,13,14</sup> and many new photocatalytic materials, such as graphitic carbon nitride (g-C<sub>3</sub>N<sub>4</sub>),<sup>15</sup> crystalline

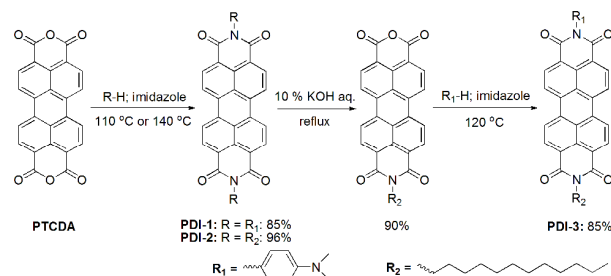
polyimides,<sup>16,17</sup> carbon materials (carbon nanotubes, graphite oxide, graphene, graphene oxide, reduced graphene oxide),<sup>18-22</sup> as well as their composites,<sup>23-26</sup> are usually produced from high energy consuming production processes which detract from the overall goal of an alternative energy system. To meet these challenges, increasing research efforts have now been put into the design and development of new photocatalyst materials (or composites), as well as the novel photocatalytic mechanisms that may lead to further improvement of the photoconversion efficiency through nanoscale structural modification.<sup>27-29</sup> Among the new materials, small molecules based on PDI show promise as efficient photocatalysts. PDI and its derivatives are well-known n-type organic semiconductors that are commonly used in organic electronics, sensitizers in dye-sensitized solar cells and as the acceptors in bulk heterojunction organic photovoltaics due to their unique optoelectronic properties.<sup>30-33</sup> They have a bandgap around 2 eV with outstanding photo-response in visible wavelengths that match well with the solar spectrum. They exhibit large exciton and charge diffusion lengths due to the extended  $\pi$ -electron delocalization through strong  $\pi$ - $\pi$  overlap.<sup>34-37</sup> Indeed, PDIs demonstrate the highest mobilities among common organic semiconductors.<sup>38</sup> Furthermore, chemical functionalization of PDIs can be used to tune the redox potentials and/or binding properties leading to efficient semiconductor heterostructures with energy levels suitable for photocatalytic-degradation or water reduction to H<sub>2</sub>.<sup>38-40</sup> Unlike most other organic molecules, PDIs have unique stability in air and under heating making them a robust material for solar energy applications.<sup>31-32</sup> Finally, in contrast to inorganic and carbonic counterparts, PDIs can be synthesized following simple synthetic

routes from low-cost and abundant materials in high yields and purity.<sup>30</sup> For these reasons, PDIs are considered to be promising materials in photocatalytic systems and have already attracted several investigations. For example, amorphous PDI was attached onto the surface of TiO<sub>2</sub> nanoparticles, or another inorganic metal oxide, mainly as a visible-light-responsive sensitizer for photo-degradation of pollutants.<sup>39,40</sup> However, the efficiency is limited largely by the inefficient charge transport in the amorphous PDI, resulting in losses before charge transfer reaction can occur at the TiO<sub>2</sub> interface.<sup>39,40</sup>



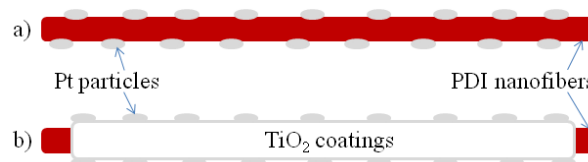
**Scheme 1** Schematic diagram for recent development (fabrication, morphology and application) of 1D self-assembly of PDIs.

In the last decade, orderly 1D nanostructures of PDIs fabricated from simple solution-phase self-assembly have been extremely attractive as building blocks for organic optoelectronic devices in line with a large number of very appealing results (Scheme 1).<sup>41-47</sup> Strong  $\pi$ - $\pi$  stacking of the large and flat aromatic core of PDI drives the self assembly process. In comparison with the single-molecule and bulk-phase PDIs, well-defined PDI-nanofibers exhibit high purity, more efficient photo-induced exciton generation and dissociation and higher electron mobility along the  $\pi$ - $\pi$  stacking direction. The high mobility along the stacking direction makes PDI nanofibers a common material in OFET applications. The large surface area and reactivity of the PDI fibers give them a unique advantage for chemical sensors through interfacial charge transfer.<sup>33</sup> Furthermore, 1D PDI-based heterostructures can be fabricated with organic or inorganic materials to form nanoscale p-n junctions for large area and efficient photovoltaic cells.<sup>48,49</sup> Combination of the large surface area, enhanced charge separation and high surface reactivity to form a large number of nano-composite structures makes PDI nanofibers a very promising system for photocatalytic activity. While PDI sensitized composites have been studied for photocatalytic applications,<sup>50</sup> there has been little investigation on the 1D self-assembly of PDIs for water splitting applications, to the best of our knowledge.



**Scheme 2** Synthetic routes of PDI-based molecules.

In this study, we prepared a series PDI nanofibers coated with co-catalyst Pt and/or TiO<sub>2</sub> to study the effect of nanomorphology on photocatalytic water splitting for hydrogen generation under visible-light irradiation. Three PDI-based molecules (PDI-1 to PDI-3; Scheme 2) attached with either an inert dodecyl chain or electron-donating N,N-dimethylaniline group were used for comparative investigation of the effect of side-chain modification on nanofiber growth and catalytic activity.<sup>30,38,51-53</sup> The molecules were either symmetric (PDI-1, PDI-2) or asymmetric (PDI-3) leading to different stacking orientations and ultimately different nanomorphologies. Co-catalyst Pt and/or TiO<sub>2</sub> were deposited on the PDI nanofibers through a facile in-situ solution deposition to form 1D hybrid nanocomposites (Scheme 3).<sup>2,27,54</sup> A sacrificial electron donor molecule of CH<sub>3</sub>OH or triethanolamine (TEA) was used to facilitate the H<sub>2</sub> generation. Complete experimental details, including material synthesis, characterization, and photocatalytic tests, are available in the supporting information.



**Scheme 3** Schematic diagram of 1D hybrid nanocomposites: a) Pt/PDI-X nanofibers fabricated by in-situ deposition of Pt on PDI-X nanofibers; b) Pt/TiO<sub>2</sub>/PDI-X nanofibers fabricated by in-situ deposition of TiO<sub>2</sub> and then Pt on PDI-X nanofibers.

## Results and discussion

### Molecular characterization

The PDI molecules 1-3 were chosen to optimize both self-assembly and photocatalytic activity through side chain modification. The dodecyl chain (R<sub>2</sub>) was used to improve solubility in CHCl<sub>3</sub> for enhanced self assembly process. Conversely, the aniline functional group (R<sub>1</sub>) acts as an electron donor to effectively increase intramolecular charge separation under illumination, aiming to promote the photocatalytic activity. Substitution at the imide position of PDI more or less influences the thermodynamic stability (Fig. S1) but should not result in modification of the molecular orbitals due to a node in the highest occupied molecular orbital (HOMO) and the lowest unoccupied molecular orbital (LUMO) at the imide.<sup>30,33,55</sup> Indeed, functionalization for all PDI molecules showed no significant change in the molecular energy levels as determined from optical spectroscopy (Fig. S2) and cyclic voltammetry (Table S1). Thus, major differences in H<sub>2</sub> generation across the three PDIs can be

attributed to differences in molecular packing, nanoscale morphology, and intramolecular charge separation efficiency.

### Nanoscale self-assembly

Nanofibers of PDIs were fabricated through solution phase self-assembly, which was performed via bisolvent interfacial transfer of PDIs.<sup>33,53</sup> Briefly, a large volume of a poor solvent, CH<sub>3</sub>OH, was injected slowly into a small volume of high concentrations of PDI in a good solvent, CHCl<sub>3</sub>. Self-assembly occurs as the solubility of PDI decreases in the mixture solvent, mainly driven by the strong intrinsic co-facial  $\pi$ - $\pi$  stacking of the aromatic core in the long axis of the nanostructure, in conjunction with the hydrophobic association between the side chains along in the short axis.<sup>6,32,40</sup> Thus, there are several degrees of freedom in the fabrication method to control the nanostructure morphology, such as solubility in different solvents and aging conditions. In this study, all PDI samples formed well-defined nanofiber structures through a slow injection technique where 400 mL of CH<sub>3</sub>OH was slowly added dropwise to 100 mL of CHCl<sub>3</sub> (100  $\mu$ mol L<sup>-1</sup>) solution followed by aging for 24 h at room temperature. This slow injection technique produces a more thermodynamically stable structure. Fig. 1 shows the different nanomorphologies obtained with the three different PDI molecules using the slow injection technique. PDI-1 and PDI-2 formed short nanorods and long nanobelts respectively, whereas PDI-3 produced longer but thicker nanowires (several to tens of microns long). Alternatively, a quick injection and dispersion method was also employed which forms shorter and less ordered nanostructures of PDI-3 (Fig. S5).<sup>56</sup> All of the PDI nanostructures were very stable in solution and could be transferred to polar or nonpolar solid surfaces for further characterization and functionalization. Despite the different nanomorphologies, all PDI nanostructures form extended 1D charge carrier pathways, large surface area for high reactivity and long term stability, making them all suitable for comparative photocatalytic experiments.

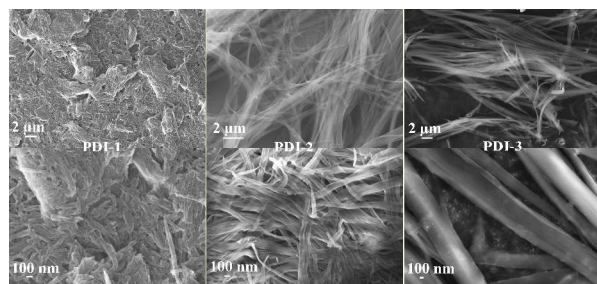


**Fig. 1** SEM images of nano-assemblies fabricated from PDIs at low (up) and high (down) magnification.

### Preparation of nanocomposites

To realize a functional photocatalytic system, nanocomposites (Scheme 3) composed of PDI nanofibers coated with co-catalysts Pt and TiO<sub>2</sub> were fabricated. TiO<sub>2</sub> was employed as electron transfer relay that accepts electron from PDI and transfers it to Pt, which provides active sites for reduction of water to H<sub>2</sub>. Such TiO<sub>2</sub> mediated electron transfer helps suppress the electron-hole recombination. The expected photocatalytic mechanism is shown in Scheme 4. In this system, PDIs are used as central

photocatalyst that responds to visible light (Fig. S3). Photo-excitation of PDI promotes electron transition from the HOMO to the LUMO, leaving a hole (positive charge) located at HOMO. For PDI-1 and PDI-3, which are both attached with aniline group (a strong electron donor), rapid intramolecular electron transfer from aniline can fill in the hole, i.e., neutralize the positive charge, producing a long-range (thus long lived) charge separation between the PDI backbone and aniline substituent. Further, 1D organized  $\pi$ - $\pi$  stacking between PDI molecules enables extensive delocalization of the electron along the long axis of nanofiber (a band like charge transport process).<sup>33,38</sup> This intermolecular charge delocalization not only suppresses the charge recombination, but more importantly enhances the interfacial electron capture by TiO<sub>2</sub>. In the presence of sacrificial donor reagent, such as CH<sub>3</sub>OH or TEA, the positive charge at the aniline moiety can be effectively scavenged (neutralized), thus allowing for continuous flow of electrons along the nanofibers. In comparison, for PDI-2, which is not connected with an electron donor, the hole left in the HOMO of PDI can only be scavenged by the sacrificial reducing reagent, an intermolecular process that is much less efficient than the intramolecular electron transfer from aniline to PDI as in the case of PDI-1 or PDI-3. This means that the electron-hole recombination within PDI-2 would strongly competes with the interfacial electron transfer from PDI to TiO<sub>2</sub>, leading to decreased photocatalysis efficiency as observed in Fig. 2 and 3.

To examine the role of 1D nanomorphology of PDI, photocatalytic reduction of water was investigated with both PDI sensitized Pt/TiO<sub>2</sub> nano-particle composites and Pt/TiO<sub>2</sub> coated PDI nanofiber composites. Commercially available P25 TiO<sub>2</sub> nanoparticles were used for fabricating the PDI sensitized nanocomposites (see Supporting Information for experimental detail), here to be referred as PDI-X/Pt/P25. For the Pt/TiO<sub>2</sub> coated PDI nanofiber composites, here to be referred as Pt/TiO<sub>2</sub>/PDI-X. TiO<sub>2</sub> was first deposited on the PDI nanofiber surface by reduction of titanium isopropoxide in a PDI nanofiber solution of CHCl<sub>3</sub>/CH<sub>3</sub>OH. Pt nanoparticles were deposited onto either P25 TiO<sub>2</sub> nanoparticles, TiO<sub>2</sub> coated PDI nanofibers or bare PDI nanofibers by in-situ photo-reduction from H<sub>2</sub>PtCl<sub>6</sub>•6H<sub>2</sub>O in an aqueous solution. The in-situ deposition of TiO<sub>2</sub> and Pt onto PDI fibers was proven to not damage the PDI nanomorphology as seen in Fig. S6 and S7.

For efficient photocatalytic systems, the catalyst should be well dispersed and stable in the aqueous solvent. The presence of the PDI molecules allow for improved dispersion of the sensitized Pt/P25 nanocomposites in aqueous solution compared to pristine TiO<sub>2</sub> nanoparticles. Conversely, TiO<sub>2</sub> coating on PDI nanofiber surface acts as a protective layer to improve the mechanical and chemical stability of the long and flexible PDI nanofibers in solution during the photocatalytic tests. To maintain good dispensability and avoid clumping of PDI nanofibers during the in-situ hydrolysis process, an optimized weight ratio 5 wt.% of TiO<sub>2</sub> to PDI nanofibers was determined (Fig. S9).

### Photocatalytic H<sub>2</sub> production

The presence of sacrificial reagents and noble-metal Pt was found necessary for efficient H<sub>2</sub> generation under visible-light ( $\lambda > 420$  nm) irradiation.<sup>2,54</sup> In this work, 0.5 wt.% of co-catalyst Pt to



TiO<sub>2</sub> and 10 vol.% of TEA in aqueous solution were determined to be optimal (Fig. S8) and chosen for the remainder of the experiments.

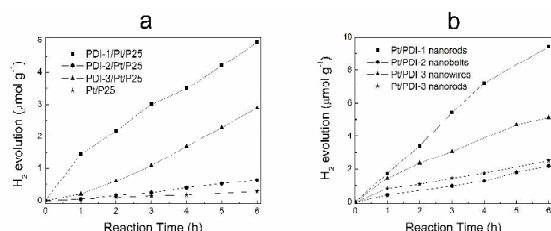


**Fig. 2** (a) The time courses of H<sub>2</sub> evolution over PDI-X(0.5 wt.)/Pt/P25 nanoparticles and (b) Pt(0.5 wt.)/PDI-X nanofibers with TEA (10 vol.%) as the sacrificial reagent.

As shown in Fig. 2a, PDI-sensitization of all three molecules on Pt(0.5 wt.)/P25 nanoparticles enhanced H<sub>2</sub> generation from water. This enhancement is attributed to increased visible light absorption. Among these PDIs, however, PDI-1 exhibits the highest performance followed by PDI-3. PDI-1 and PDI-3 molecules both contain the aniline functional group, which acts as an intramolecular electron donor.<sup>38</sup> In bicomponent system of PDI nanofibers coated with Pt co-catalyst, similar results are obtained, as shown in Fig. 2b, where the H<sub>2</sub> generation rate of Pt(0.5 wt.)/PDI-1 nanofibers is more than double that of the other PDI systems. Thus, it is hypothesized that the intramolecular electron transfer from aniline to PDI enhances the photocatalytic activity as illustrated in Scheme 4. In addition, the better photocatalytic performance of Pt/PDI-X nanofibers than PDI-X/Pt/P25 nanoparticles is largely due to the nanofiber morphology that possesses extended  $\pi$ - $\pi$  stacking structure enabling efficient charge transfer and separation in the former system as discussed above, whereas in the later, the weak physical adsorption between PDI-X and Pt/P25 particle results in inferior interfacial charge transfer and separation.

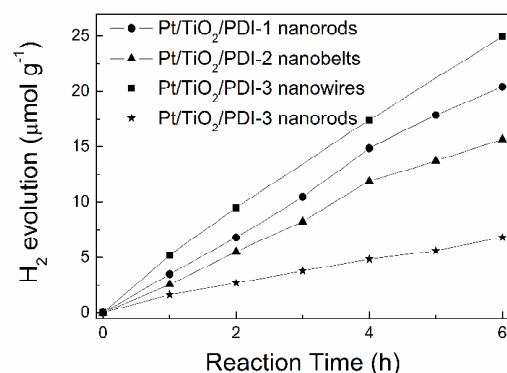


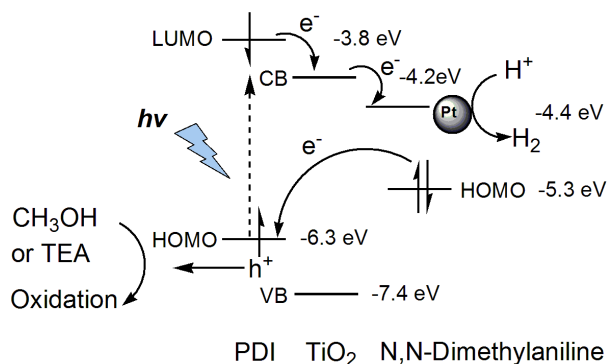
**Fig. 3** The time courses of H<sub>2</sub> evolution over Pt(0.5 wt.)/TiO<sub>2</sub>(5 wt.)/PDI-X nanofiber composites using TEA (10 vol.%) as the sacrificial reagent.

TiO<sub>2</sub> was coated on the surface of the PDI nanofibers to enhance photocatalytic activity through interfacial charge separation. The weight ratio of TiO<sub>2</sub> to PDI nanofiber was optimized to balance surface coverage and dispensability. An optimized photocatalyst material was found to be Pt(0.5 wt.)/TiO<sub>2</sub>(5 wt.)/PDI-3 nanofiber (Fig. S9). This material was capable of producing 100

$\mu\text{mol g}^{-1}$  H<sub>2</sub> within 24 h. Unlike the experiments shown in Fig. 2 (where the photocatalysis performance of PDI-1 is better than that of PDI-3), here PDI-3-based nanocomposites showed a better result than that of PDI-1 (Fig. 3). Based on the SEM imaging (Fig. 1), it can be seen that the PDI-3 nanofibers formed a longer and more ordered nanostructure compared to PDI-1. Therefore, it is hypothesized that the improved nanomorphology enhanced the photocatalytic activity. To further test this, PDI-3 nanorods fabricated through the fast injection technique (Fig. S5) was investigated for the same photocatalysis as comparison. As expected, the short nanorods demonstrated much lower efficiency of H<sub>2</sub> production under the same photoreaction conditions (Fig. 3).

## Mechanism speculation

To explain the superior performance of the Pt/TiO<sub>2</sub>/PDI-3 nanofiber system, both the nanomorphology and molecular design are taken into consideration. By looking at only the nanomorphology, as seen in the SEM images in Fig. 1, PDI-2 nanoribbons show the highest aspect ratio, and thus largest surface area. Based on nanomorphology alone, PDI-2 should show the best performance. However, the shorter PDI-1 nanorods and thicker PDI-3 nanofibers outperform PDI-2 by nearly 25%. It is speculated that intramolecular charge transfer from the electron rich amine group is responsible for the performance enhancement by suppressing the electron-hole recombination, despite the inferior nanomorphology. Furthermore, by optimizing both nanomorphology and molecular design with the asymmetric PDI-3 system, another nearly 25% performance enhancement was obtained. This optimized design takes advantage of both intra- and inter-molecular charge transfer to promote H<sub>2</sub> generation by suppressing the back charge recombination.



**Scheme 4** Proposed photocatalytic H<sub>2</sub> evolution mechanism for Pt/TiO<sub>2</sub>/PDI-1(3) nanofiber composites, for which the hole left in the HOMO of PDI can be filled in by rapid intramolecular electron transfer from the aniline group. For PDI-2, which is not attached with an electron donor, the hole can be scavenged by the sacrificial reducing reagent. Energy values (vs. vacuum level) are taken from references given in the article.

Indeed, the mechanism illustrated in Scheme 4 also explains why PDI-1 outperforms PDI-3 in the bicomponent system with no TiO<sub>2</sub> deposition (Fig. 2b). When no TiO<sub>2</sub> is present, the energy level alignment between the LUMO of the PDI and work function of the Pt is poor suggesting slow electron transfer. The extended

charge carrier lifetime stemming from the larger  $\pi$ - $\pi$  system in PDI-3 may not be enough to suppress the charge carrier recombination. Therefore, the overall photocatalysis becomes mostly determined by the intramolecular electron transfer from the aniline group to PDI, for which the positive charge formed at the aniline can be neutralized by reacting with the sacrificial reagent. Since PDI-1 has two aniline groups, its photocatalytic performance is increased.

## Conclusions

To sum up, Pt and/or TiO<sub>2</sub> deposited nanofibers of three PDI derivatives have been developed as novel photocatalysts for H<sub>2</sub> production from water-splitting under visible light irradiation. Optimization of both molecular design and nanomorphology was performed. In short, the intramolecular donor-acceptor structure of asymmetric PDI-3 molecule together with extended intermolecular electron delocalization along the long axis of its nanofibers accounts for their better performance than others. Although the present hydrogen evolution efficiency of these composites is still far from practical need, the primary work demonstrates a new strategy to develop high performance organic or organic-inorganic photocatalysts, which provide numerous options to optimize the property and function at nanoscale. In the future, inspired by the present results, more suitable PDI molecules with selective donor moieties will be studied to satisfy the needs of controllable 1D self-assembly and adjustable composite fabrication. Similarly, the energy level difference between the HOMO of PDIs and conduction band of TiO<sub>2</sub> or Fermi level of Pt should be critically considered to achieve much improved charge separation. Moreover, more promising results are anticipated by introducing well-tailored supramolecular nanostructures of bay-substituted or core-extended PDIs (donor-acceptor type having hydrophobic/hydrophilic characteristics), as well as constructing organic nanofiber based hybrid nanocomposites like p/n heterostructures or co-assembled crystalline donor-acceptor heterojunctions.

## Acknowledgements

Financial support by the National Natural Science Foundation of China (Grant No. 21173261), the "One Hundred Talents" program of Chinese Academy of Sciences, and the "Cross Cooperation Program for Creative Research Teams" of Chinese Academy of Sciences is gratefully acknowledged.

## Notes and references

<sup>a</sup> Laboratory of Environmental Sciences and Technology, Xinjiang Technical Institute of Physics & Chemistry; Key Laboratory of Functional Materials and Devices for Special Environments, Chinese Academy of Sciences, Urumqi, 830011, China. Fax: (86)991-3838957; Tel: (86)991-3835879; E-mail: cywang@ms.xjb.ac.cn (C. Wang)

<sup>b</sup> The Graduate School of Chinese Academy of Science, Beijing, 100049, China.

<sup>c</sup> NanoInstitute of Utah and Department of Materials Science and Engineering, University of Utah, Salt Lake City, UT, 84112, US. E-mail: lzang@eng.utah.edu (L. Zang)

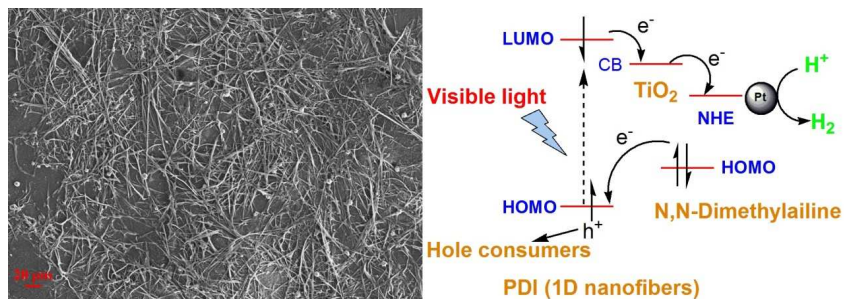
† Electronic Supplementary Information (ESI) available: Experimental details, Table S1 and Fig. S1–S9. See DOI: 10.1039/b000000x/

1 M. Ashokkumar, *Int. J. Hydrogen Energy*, 1998, **23**, 427.

- 2 M. Ni, M. K. H. Leung, D. Y. C. Leung, K. Sumathy, *Renew. Sust. Energ. Rev.*, 2007, **11**, 401.
- 3 A. Kudo, Y. Miseki, *Chem. Soc. Rev.*, 2009, **38**, 253.
- 4 X. B. Chen, S. H. Shen, L. J. Guo, S. S. Mao, *Chem. Rev.*, 2010, **110**, 6503.
- 5 M. Cargnello, B. T. Diroll, *Nanoscale*, 2014, **6**, 97.
- 6 T. Hisatomi, J. Kubota, K. Domen, *Chem. Soc. Rev.*, 2014, DOI: 10.1039/C3CS60378D.
- 7 N. Skillen, C. McCullagh, M. Adams, *Environmental Photochemistry Part III, Hdb Env. Chem.*, DOI 10.1007/698\_2014\_261.
- 8 J. R. McKone, N. S. Lewis, H. B. Gray, *Chem. Mater.*, 2014, **26**, 407.
- 9 G. C. Dismukes, *Science*, 2001, **292**, 447.
- 10 Z. J. Han, F. Qiu, R. Eisenberg, P. L. Holland, T. D. Krauss, *Science*, 2012, **338**, 1321.
- 11 D. L. Lu, T. Takata, N. Saito, Y. Inoue, K. Domen, *Nature*, 2006, **440**, 295.
- 12 C. E. Nebel, *Nat. Mater.*, 2013, **12**, 780.
- 13 W. J. Youngblood, S. A. Lee, K. Maeda, T. E. Mallouk, *Acc. Chem. Res.*, 2009, **42**, 1966.
- 14 Y. H. Hu, *Angew. Chem. Int. Ed.*, 2012, **51**, 12410.
- 15 X. C. Wang, K. Maeda, A. Thomas, K. Takanabe, G. Xin, J. M. Carlsson, K. Domen, M. Antonietti, *Nat. Mater.*, 2009, **8**, 76.
- 16 S. Chu, Y. Wang, Y. Guo, P. Zhou, H. Yu, L. L. Luo, F. Kong, Z. G. Zou, *J. Mater. Chem.*, 2012, **22**, 15519.
- 17 S. Chu, Y. Wang, C. C. Wang, J. C. Yang, Z. G. Zou, *Int. J. Hydrogen Energy*, 2013, **38**, 10768–10772.
- 18 T. F. Yeh, J. M. Syu, C. Cheng, T. H. Chang, H. Teng, *Adv. Funct. Mater.*, 2010, **20**, 2255.
- 19 Q. J. Xiang, J. G. Yu, M. Jaroniec, *Chem. Soc. Rev.*, 2012, **41**, 782.
- 20 N. Zhang, Y. H. Zhang, Y. J. Xu, *Nanoscale*, 2012, **4**, 5792.
- 21 Q. J. Xiang, J. G. Yu, *J. Phys. Chem. Lett.*, 2013, **4**, 753.
- 22 X. Q. An, J. C. Yu, *RSC Adv.*, 2011, **1**, 1426.
- 23 B. Chai, T. Y. Peng, J. Mao, K. Li, L. Zan, *Phys. Chem. Chem. Phys.*, 2012, **14**, 16745.
- 24 X. J. Lv, W. F. Fu, H. X. Chang, H. Zhang, J. S. Cheng, G. J. Zhang, Y. Song, C. Y. Hu, J. H. Li, *J. Mater. Chem.*, 2012, **22**, 1539.
- 25 L. Han, P. Wang, S. J. Dong, *Nanoscale*, 2012, **4**, 5814.
- 26 R. Marschall, *Adv. Funct. Mater.*, 2014, **24**, 2421.
- 27 S. U. M. Khan, M. Al-Shahry, W. B. I. Jr, *Science*, 2002, **297**, 2243.
- 28 S. M. Ji, H. Jun, J. S. Jang, H. C. Son, P. H. Borse, J. S. Lee, *J. Photochem. Photobiol. A*, 2007, **189**, 141.
- 29 X. B. Chen, L. Liu, P. Y. Yu, S. S. Mao, *Science*, 2011, **331**, 746.
- 30 C. Huang, S. Barlow, S. R. Marder, *J. Org. Chem.*, 2011, **76**, 2386.
- 31 C. Li, H. Wonneberger, *Adv. Mater.*, 2012, **24**, 613.
- 32 E. Kozma, M. Catellani, *Dyes Pigments*, 2013, **98**, 160.
- 33 L. Zang, Y. Che, J. S. Moore, *Acc. Chem. Res.*, 2008, **41**, 1596.
- 34 Y. Che, H. L. Huang, M. Xu, C. Y. Zhang, B. R. Bunes, X. M. Yang, L. Zang, *J. Am. Chem. Soc.*, 2011, **133**, 1087.
- 35 D. Chaudhuri, D. B. Li, Y. Che, E. Shafran, J. M. Gerton, L. Zang, J. M. Lupton, *Nano Lett.*, 2011, **11**, 488.
- 36 Y. L. Chen, L. N. Chen, G. J. Qi, H. X. Wu, Y. X. Zhang, L. Xue, P. H. Zhu, P. Ma, X. Y. Li, *Langmuir*, 2010, **26**, 12473.
- 37 L. N. Zhong, F. F. Xing, W. Shi, L. M. Yan, L. Q. Xie, S. R. Zhu, *ACS Appl. Mater. Interfaces*, 2013, **5**, 3401.
- 38 Y. Che, X. M. Yang, G. L. Liu, C. Yu, H. W. Ji, J. M. Zuo, J. C. Zhao, L. Zang, *J. Am. Chem. Soc.*, 2010, **132**, 5743.
- 39 A. Senthilraja, B. Krishnakumar, M. Swaminathan, S. Nagarajan, *New J. Chem.*, 2014, **38**, 1573.
- 40 J. T. Kirner, J. J. Stracke, B. A. Gregg, R. G. Finke, *ACS Appl. Mater. Interfaces*, 2014, DOI: 10.1021/am405598w.
- 41 J. A. A. W. Elemans, R. van Hameren, R. J. M. Nolte, A. E. Rowan, *Adv. Mater.*, 2006, **18**, 1251.
- 42 M. Hasegawa, M. Iyoda, *Chem. Soc. Rev.*, 2010, **39**, 2420.
- 43 C. Li, H. Wonneberger, *Adv. Mater.*, 2012, **24**, 613.
- 44 D. Görl, X. Zhang, F. Würthner, *Angew. Chem. Int. Ed.*, 2012, **51**, 6328.
- 45 L. Xu, M. Hirono, T. Seki, H. Kurata, T. Karatsu, A. Kitamura, D. Kuzuhara, H. Yamada, T. Ohba, A. Saeki, S. Seki, S. Yagai, *Chem. Eur. J.*, 2013, **19**, 6561.
- 46 M. Supura, S. Fukuzumi, *ECS J. Solid State Sci. Tech.*, 2013, **2**, M3051.

- 47 W. Yao, Y. S. Zhao, *Nanoscale*, 2014, **6**, 3467.
- 48 J. T. Kirner, J. J. Stracke, B. A. Gregg, R. G. Finke, *ACS Appl. Mater. Interfaces*, 2014, DOI: 10.1021/am405598w.
- 49 Z. X. Zhang, H. L. Huang, X. M. Yang, L. Zang, *J. Phys. Chem. Lett.*, 2011, **2**, 2897.
- 50 F. S. Liu, R. Ji, M. Wu, Y. M. Sun, *Acta Phys. Chim. Sin.*, 2007, **23**, 1899.
- 51 Y. W. Huang, L. N. Fu, W. J. Zou, F. L. Zhang, Z. X. Wei, *J. Phys. Chem. C*, 2011, **115**, 10399.
- 10 52 G. Boobalan, P. K. M. Imran, C. Manoharan, S. Nagarajan, *J. Colloid Interface Sci.*, 2013, **393**, 377.
- 53 K. Balakrishnan, A. Datar, T. Naddo, J. L. Huang, R. Oitker, M. Yen, J. C. Zhao, L. Zang, *J. Am. Chem. Soc.*, 2006, **128**, 7390.
- 54 J. H. Yang, D. G. Wang, H. X. Han, C. Li, *Acc. Chem. Res.*, 2013, **46**, 1900.
- 15 55 R. C. Liu, M. W. Holman, L. Zang, D. M. Adams, *J. Phys. Chem. A*, 2003, **107**, 6522.
- 56 K. Balakrishnan, A. Datar, R. Oitker, H. Chen, J. M. Zuo, L. Zang, *J. Am. Chem. Soc.*, 2005, **127**, 10496.
- 20

## Graphical Abstract



## Highlights

Self-assembled 1D nanofibers of donor-accepter type perylene diimides have been used for photocatalytic  $\text{H}_2$  production from water-splitting under visible-light irradiation.